doi:10.1016/j.jmb.2011.02.049 J. Mol. Biol. (2011) 408, 780–791

Contents lists available at www.sciencedirect.com

Journal of Molecular Biology

journal homepage: http://ees.elsevier.com.jmb

The Osaka FAD Mutation E22Δ Leads to the Formation of a Previously Unknown Type of Amyloid β Fibrils and Modulates Aβ Neurotoxicity

Oxana Yu. Ovchinnikova[1]†, Verena H. Finder[1,2]†, Ivana Vodopivec[2]†, Roger M. Nitsch[2] and Rudi Glockshuber[1]*

[1]*Institute of Molecular Biology and Biophysics, ETH Zurich, Schafmattstrasse 20, CH-8093 Zurich, Switzerland*
[2]*Division of Psychiatry Research, University of Zurich, August Forel Strasse 1, 8008 Zurich, Switzerland*

Received 10 September 2010; received in revised form 7 February 2011; accepted 19 February 2011
Available online 12 March 2011

Edited by S. Radford

Keywords:
Aβ;
Alzheimer's disease;
E22Δ;
aggregation;
neurotoxicity

Alzheimer's disease (AD) is a neurodegenerative disorder characterized by cerebral deposition of amyloid fibrils formed by the amyloid β (Aβ) peptide. Aβ has a length of 39–43 amino acid residues; the predominant Aβ isoforms are Aβ1–40 and Aβ1–42. While the majority of AD cases occur spontaneously, a subset of early-onset familial AD cases is caused by mutations in the genes encoding the Aβ precursor protein or presenilin 1/presenilin 2. Recently, a deletion of glutamic acid at position 22 within the Aβ sequence (E22Δ) was identified in Japanese patients with familial dementia, but the aggregation properties of the deletion variant of Aβ are not well understood. We investigated the aggregation characteristics and neurotoxicity of recombinantly expressed Aβ isoforms 1–40 and 1–42 with and without the E22Δ mutation. We show that the E22Δ mutation strongly accelerates the fibril formation of Aβ1–42 E22Δ compared to Aβ1–42 wild type (wt). In addition, we demonstrate that fibrils of Aβ1–40 E22Δ form a unique quaternary structure characterized by a strong tendency to form fibrillar bundles and a strongly increased thioflavin T binding capacity. Aβ1–40 E22Δ was neurotoxic in rat primary neuron cultures as compared to nontoxic Aβ1–40 wt. Aβ1–42 E22Δ was less toxic than Aβ1–42 wt, but it significantly decreased neurite outgrowth per cell in neuronal primary cultures. Because Aβ1–40 is the major Aβ form *in vivo*, the gain of toxic function caused by the E22 deletion may explain the development of familial AD in mutation carriers.

*Corresponding author. E-mail address: rudi@mol.biol.ethz.ch.

† O.Y.O., V.H.F., and I.V. contributed equally to this work.

Present address: I. Vodopivec, Boston University Medical Center, 72 East Concord Street, Evans 124, Boston, MA 02118, USA.

Abbreviations used: AD, Alzheimer's disease; Aβ, amyloid β; wt, wild type; APP, amyloid precursor protein; FAD, familial AD; PIB, Pittsburgh compound B; LDH, lactate dehydrogenase; [^{11}C]PIB, [^{11}C]Pittsburgh compound B; 6-OH-BTA-1, 6-benzothiazolol; ACN, acetonitrile; DMSO, dimethyl sulfoxide; DAPI, 4′,6-diamidino-2-phenylindole.

Introduction

According to the amyloid hypothesis, aggregation of the amyloid β (Aβ) peptide and accumulation in extracellular deposits in the neuropil and in the cerebral vasculature are central events in the pathophysiology of Alzheimer's disease (AD), which is the most prevalent neurodegenerative disease in the growing population of elderly people.[1] Aβ has a length of 39–43 amino acid residues and is generated from the amyloid precursor protein (APP) via endoproteolytic cleavage by β-secretase and γ-secretase[2] (Fig. 1). Two major Aβ isoforms are produced in the human brain: Aβ1–40 and Aβ1–42. The longer Aβ1–42 peptide is present

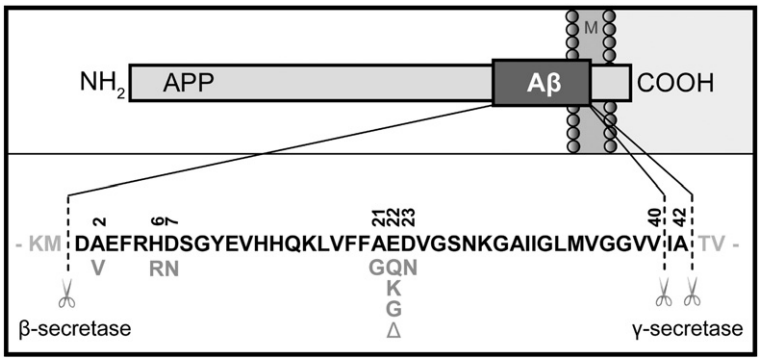

Fig. 1. Schematic diagram of the APP highlighting known mutations within the Aβ sequence that are linked with FAD. The gray letters below the Aβ sequence indicate the known missense mutations within the Aβ sequence: A2V, English (H6R), Tottori (D7N), Flemish (A21G), Dutch (E22Q), Italian (E22K), Arctic (E22G), Osaka (E22Δ), and Iowa (D23N). The main cleavage sites of β-secretase and γ-secretase are indicated with broken lines and scissors. M: membrane.

in the brain at approximately 10% of the concentration of Aβ1–40,[3–5] but has a higher tendency to aggregate and form amyloid fibrils than Aβ1–40; Aβ1–42 is therefore considered as the pathologically relevant form in the pathophysiology of AD.[6]

In most AD cases, the disease occurs spontaneously, with late onset. However, a small number of AD cases have a familial background and are frequently associated with a lower age of onset. Familial AD (FAD) can be caused by mutations in the genes encoding APP or presenilin 1/presenilin 2.[7,8] Some of the mutations in the gene encoding APP affect the sequence of Aβ itself, including the so-called Flemish (A21G),[9] Dutch (E22Q),[10] Italian (E22K),[11] Arctic (E22G),[12] Iowa (D23N),[13] Tottori (D7N),[14] English (H6R),[15] and A2V[16] mutations, which were all found to cause familial forms of dementia associated with amyloid deposition (Fig. 1). The clustering of mutations around positions 21–23 within the Aβ sequence may suggest a particular susceptibility to altered Aβ properties, as most of the corresponding Aβ variants exhibit an increased propensity to form amyloid fibrils.[17] Recently, a further unusual mutation within this cluster—the deletion of glutamate 22—was discovered in Japanese patients.[5,18–21] Besides the recently described Aβ mutation A2V,[16] the mutation E22Δ probably represents the first described recessive mutation related to FAD, as only homozygotes showed AD or Alzheimer's-type dementia.[5] However, the number of examined individuals was limited, and one of the heterozygous E22Δ mutation carriers exhibited mild cognitive impairment, a harbinger of AD, suggesting that this mutation may act in a dose-dependent manner. The corresponding synthetic peptides Aβ1–42 E22Δ and Aβ1–40 E22Δ were reported to show an enhanced propensity to oligomerize, but completely failed to form fibrils *in vitro*.[5] Interestingly, the amyloid signal measured *in vivo* with positron emission tomography using Pittsburgh compound B (PIB) was low in a homozygous carrier of the E22Δ mutation, suggesting low concentrations of fibrils or a lower affinity of the mutant fibrils for PIB as compared to wild-type (wt) fibrils.[5] Here we addressed the biochemical properties of the peptides Aβ1–40 E22Δ and Aβ1–42 E22Δ by exclusively using highly pure, recombinant peptides instead of synthetic peptides that had been used in previous studies. We found that the deletion E22Δ did not prevent the fibrillization process. Instead, it significantly enhanced the spontaneous *in vitro* aggregation of Aβ1–42 E22Δ as compared to Aβ1–42 wt. In addition, the shorter deletion variant Aβ1–40 E22Δ formed fibrils with a quaternary structure different from that of Aβ1–40 wt, characterized by a higher thioflavin T binding capacity and a strongly increased tendency to form fibrillar bundles. Furthermore, we showed that Aβ1–40 E22Δ and Aβ1–42 E22Δ retained the ability to bind the *in vivo* amyloid staining dye PIB. In addition, Aβ1–40 E22Δ proved to be significantly more toxic in rat primary neurons than Aβ1–40 wt, which shows no toxicity towards primary neurons. The increased neurotoxicity of Aβ1–40 E22Δ may thus explain the early onset of AD caused by this mutation, as Aβ1–40 is known to be the major form of Aβ *in vivo*.[4,5]

Results

Aβ1–42 E22Δ aggregates faster than Aβ1–42 wt

To investigate the influence of the E22Δ mutation in the Aβ sequence on the intrinsic aggregation properties of Aβ, we produced highly pure, recombinant Aβ1–40 and Aβ1–42 peptides with and without the deletion E22Δ (see Materials and Methods for details). Amyloid fibril formation of the four Aβ variants at 37 °C, pH 7.4, 122 mM ionic strength, and 7.5 μM peptide concentration was initiated by a dilution of stock solutions of the soluble peptides in 10 mM NaOH with buffer and was monitored by both a fluorescence increase in the amyloid-specific dye thioflavin T at 482 nm and by a decrease in the concentration of soluble Aβ.

Thioflavin T fluorescence measurements revealed that Aβ1–42 E22Δ aggregated significantly faster than Aβ1–42 wt. While aggregation of Aβ1–42 wt

showed a lag phase of about 8 min, followed by rapid fibril growth for about 5 min (Fig. 2a), the lag phase was completely absent in the case of Aβ1–42 E22Δ, and the half-maximum thioflavin T fluorescence was reached within the first minute of the reaction (Fig. 2b). Moreover, the soluble Aβ1–42 E22Δ peptide disappeared immediately after the onset of the reaction, while Aβ1–42 wt remained soluble until the end of the aggregation lag phase (Fig. 2a and b). Aβ1–42 E22Δ thus showed a significantly higher tendency of amyloid fibril formation compared to Aβ1–42 wt.

To investigate the reason for the absence of the lag phase in the aggregation kinetics of Aβ1–42 E22Δ, we recorded the far-UV circular dichroism (CD) spectra of soluble Aβ1–42 wt and Aβ1–42 E22Δ in stock solutions in 10 mM NaOH. Whereas the spectrum of Aβ1–42 wt showed a minimum in the range of 195–200 nm, which is indicative of random-coil conformation, the spectrum of Aβ1–42 E22Δ showed a less pronounced minimum at 195–200 nm, but a more negative ellipticity above 205 nm (Fig. 2e). The spectrum of soluble Aβ1–42 E22Δ is consistent with a mixture of random-coil conformation and β-sheet conformation. As Aβ supposedly enters the fibrillization pathway upon β-structure formation, partial β-sheet conformation in soluble Aβ1–42 E22Δ at the onset of aggregation could explain the lack of a lag phase in its aggregation kinetics.

Aβ1–40 E22Δ formed amyloid fibrils with a distinct quaternary structure

We next analyzed the aggregation kinetics of recombinant Aβ1–40 wt and Aβ1–40 E22Δ (Fig. 2c and d). Aggregation of Aβ1–40 wt started after a lag phase similar to that of Aβ1–42 wt (8 min), but showed a significantly longer fibril growth phase of about 20 min compared to 5 min for Aβ1–42 wt

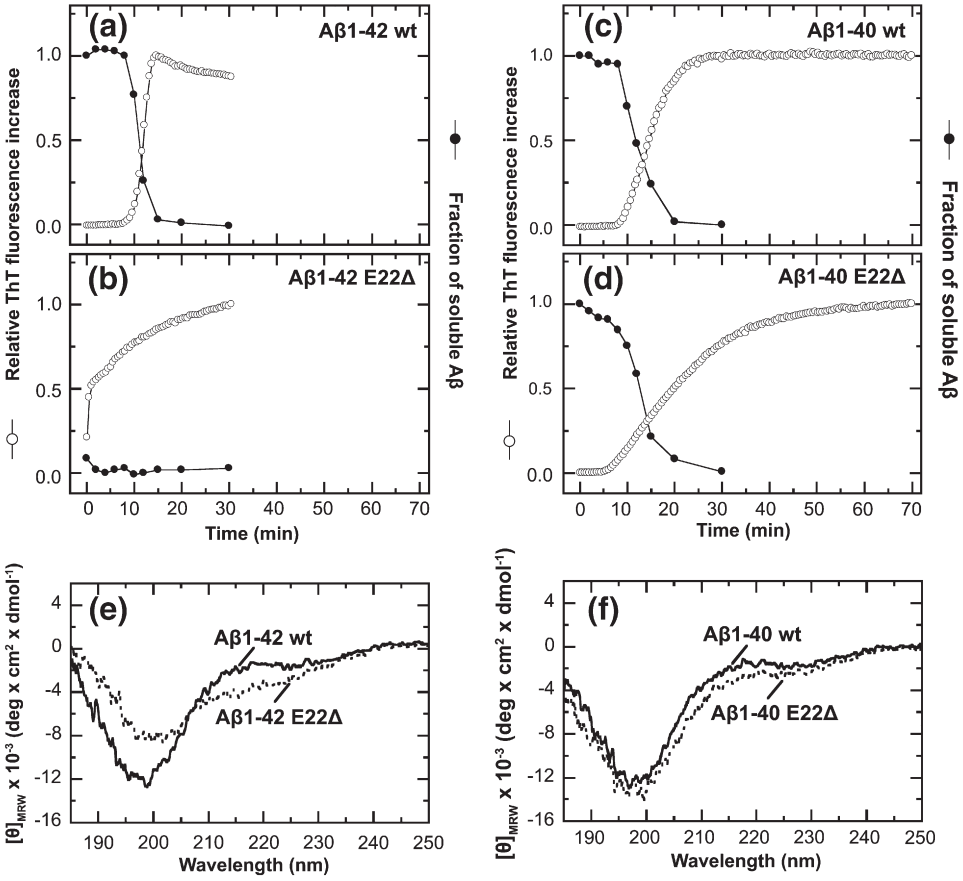

Fig. 2. Kinetics of the *in vitro* fibril formation of Aβ1–42 wt (a), Aβ1–42 E22Δ (b), Aβ1–40 wt (c), and Aβ1–40 E22Δ (d), measured via the relative increase in thioflavin T fluorescence at 482 nm (open circles) and the decrease in soluble Aβ (filled circles) during aggregation. Aggregation of the Aβ peptides (identical total monomer concentrations: 7.5 μM) at pH 7.4 and 37 °C was initiated by a 10-fold dilution of Aβ stock solutions in 10 mM NaOH with buffer. Soluble Aβ was quantified by quenching of the reactions after different times by rapid cooling, followed by ultracentrifugation and recording of the absorbance at 220 nm of soluble Aβ in the supernatants. (e and f) Far-UV CD spectra of the wt peptides (continuous lines) and the E22Δ variants (broken lines) in 10 mM NaOH (peptide concentrations: 75 μM).

(Fig. 2a and c). Specifically, the fraction of soluble Aβ1–40 E22Δ disappeared with approximately the same rate as soluble Aβ1–40 wt (no soluble peptide after 25 min) (Fig. 2c and d, filled circles), and Aβ1–40 E22Δ only showed a slightly shorter aggregation lag phase (about 6 min relative to 8 min for Aβ1–40 wt). Consistent with the presence of the lag phase in the aggregation of Aβ1–40 wt and Aβ1–40 E22Δ, the far-UV CD spectra of both peptides before the initiation of aggregation showed random-coil conformation (Fig. 2f). Despite these similarities between Aβ1–40 wt and Aβ1–40 E22Δ, Aβ1–40 E22Δ showed unique aggregation properties that distinguish this mutant peptide from wt Aβ and other mutant Aβ variants. Compared to the normalized thioflavin T fluorescence kinetics depicted in Fig. 2a–d, Fig. 3a shows the absolute fluorescence intensities recorded in the aggregation reactions of all four peptides. It reveals that the absolute thioflavin T fluorescence at the end of the aggregation reaction reached six to seven times higher intensity values relative to all other Aβ variants (Fig. 3a), and that thioflavin T fluorescence indeed increased faster in the case of Aβ1–40 E22Δ compared to Aβ1–40 wt (which is not directly evident from the normalized fluorescence data shown in Fig. 2d). Despite this faster increase in absolute thioflavin T fluorescence, the overall duration of the thioflavin T fluorescence increase was about 60 min for Aβ1–40 E22Δ compared to 20 min for Aβ1–40 wt (Figs. 2c and d and 3a). Specifically, thioflavin T fluorescence still increased significantly after 30 min when soluble Aβ1–40 E22Δ had disappeared completely (Figs. 2d and 3a), while the maximum thioflavin T fluorescence was reached after 30 min in the case of Aβ1–40 wt.

We next recorded the fluorescence emission spectra of thioflavin T bound to the four different Aβ fibrils. Samples were taken at the time point when the maximum thioflavin T fluorescence had been reached during aggregation (Fig. 3b, inset). The normalized emission spectra (Fig. 3b) show that the thioflavin T fluorescence maximum in Aβ1–40 E22Δ fibrils (475 nm) is significantly blueshifted by about 11 nm relative to that of thioflavin T bound to fibrils of Aβ1–40 wt, Aβ1–42 wt, and Aβ1–42 E22Δ, which shows a fluorescence maximum at 486 ± 1 nm. In summary, the data show that fibrils of Aβ1–40 E22Δ possess a quaternary structure that is distinct from the fibrils of Aβ1–40 wt, Aβ1–42 wt, and Aβ1–42 E22Δ, characterized by a higher thioflavin T binding capacity and/or a higher fluorescence yield of fibril-bound thioflavin T and more hydrophobic thioflavin T binding sites.

To gain insight into the differences between wt and mutant peptides with respect to amyloid fibril morphology, we imaged the fibrils formed by each of the four Aβ peptides with negative-stain electron microscopy. Figure 4a–c shows that Aβ1–42 wt and

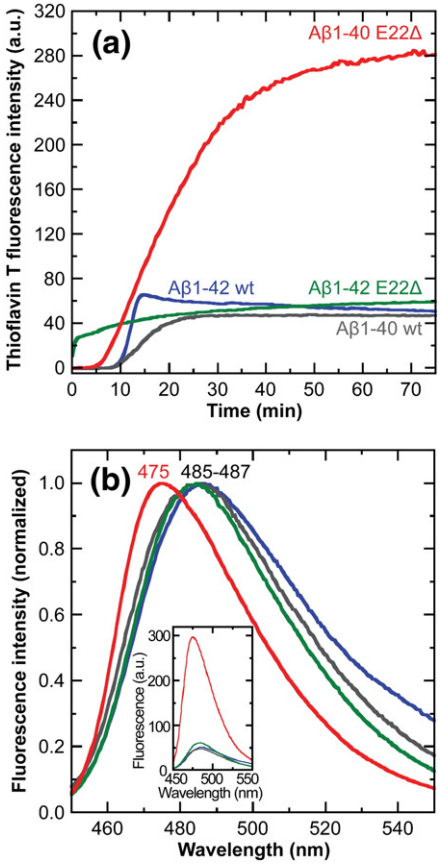

Fig. 3. (a) Kinetics of absolute thioflavin T fluorescence increase in the aggregation experiments shown in Fig. 2a–d. Fluorescence data for the aggregation of Aβ1–40 wt (gray), Aβ1–42 wt (blue), Aβ1–40 E22Δ (red), and Aβ1–42 E22Δ (green) are shown. (b) Emission spectra of fibril-bound thioflavin T (λ_{ex} = 440 nm) normalized to the respective fluorescence maximum to illustrate different spectral shapes. Fluorescence maxima are indicated with the color code from Fig. 3a. Inset: Original thioflavin T fluorescence spectra prior to normalization.

Aβ1–42 E22Δ mainly formed discrete twisted fibrils, and Aβ1–40 wt mainly formed straight fibrils that, in some cases, associated into small bundles. In contrast, Aβ1–40 E22Δ never formed discrete fibrils but exhibited a very strong tendency to form large networks of fibrillar bundles. We repeated these experiments three times and were always able to reproduce the strongly increased tendency of bundle formation of Aβ1–40 E22Δ relative to the other Aβ peptides. The fibrillar bundles of Aβ1–40 E22Δ could possibly create additional thioflavin T binding sites at the interface between individual fibrils and thus may explain their higher apparent thioflavin T binding capacity. Assuming that formation of individual fibrils precedes the formation of fibrillar bundles in the aggregation pathway of Aβ1–40 E22Δ, we speculate that the slow further

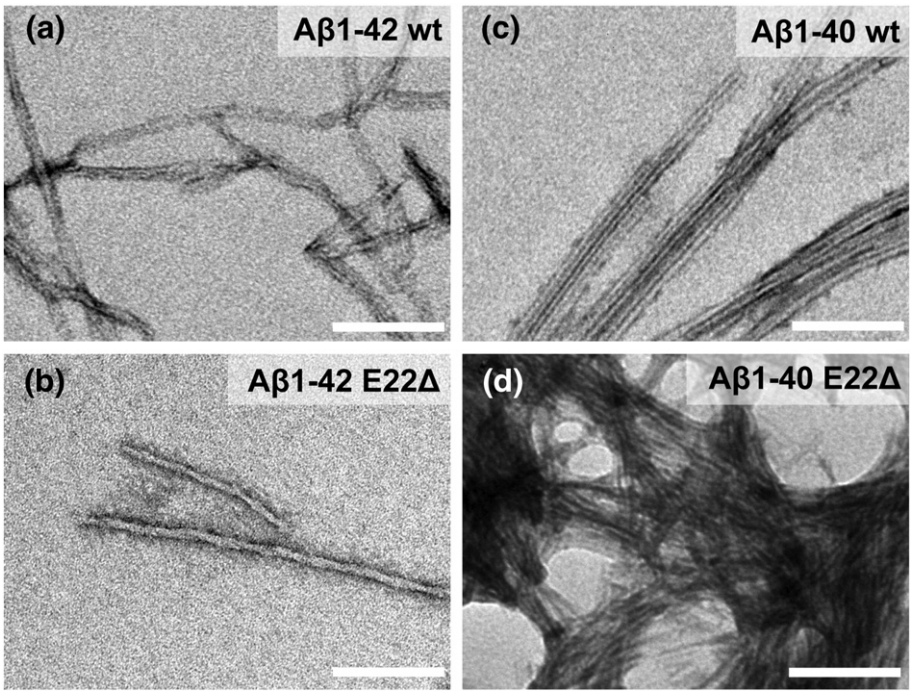

Fig. 4. Negative-stain electron micrographs of the fibrils formed by Aβ1–42 wt (a), Aβ1–42 E22Δ (b), Aβ1–40 wt (c), and Aβ1–40 E22Δ (d). A representative picture for each Aβ variant is shown (scale bar represents 100 nm).

thioflavin T fluorescence increase after the disappearance of soluble Aβ1–40 E22Δ (30–70 min after the onset of aggregation; cf. Fig. 2d) could correspond to the creation of further thioflavin T binding sites during bundle formation.

Deletion of E22 turned Aβ1–40 into a toxic peptide

To determine neurotoxicity towards the rat primary cortical neuron cultures of Aβ peptides with E22 deletion relative to wt peptides, we recorded the release of lactate dehydrogenase (LDH) from lysed cells to the culture medium after incubation for 72 h with the individual peptides (final concentrations in the growth medium: 7.5 μM) (Fig. 5). Recombinant Aβ1–42 wt or Aβ1–40 E22Δ significantly increased LDH release in comparison to vehicle controls ($P<0.001$; Tukey's test). As reported previously,[22] the longer Aβ1–42 wt peptide showed significant toxicity under these conditions, while the shorter Aβ1–40 wt peptide proved to be nontoxic. Notably, the E22 deletion in Aβ1–42 E22Δ almost completely abolished the toxicity of the longer Aβ peptide, while the deletion variant Aβ1–40 E22Δ showed significant toxicity compared to nontoxic Aβ1–40 wt. The E22 deletion thus reversed the toxicity profiles of Aβ1–40 wt and Aβ1–42 wt.

In accordance with this observation, the neuronal loss upon treatment of the primary neurons with Aβ variants was more pronounced in the case of Aβ1–42 wt and Aβ1–40 E22Δ, as judged by immunostaining of the neuronal marker MAP-2

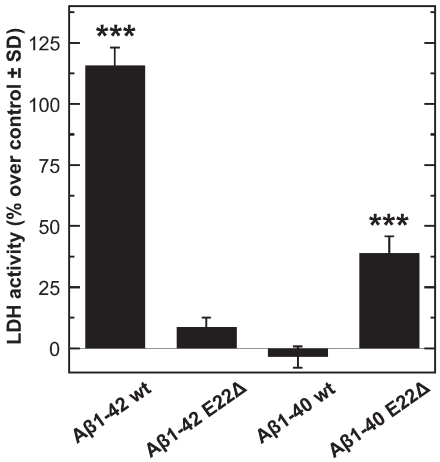

Fig. 5. Comparison of a cytotoxic effect induced by recombinant Aβ1–40 and Aβ1–42 with or without the mutation E22Δ in rat primary neuronal cell cultures. Toxicity is presented as LDH activity relative to the controls after the incubation of the cultures with the peptides for 72 h. The graph represents two independent experiments, with each bar representing the mean of four assays. Recombinant Aβ1–42 wt and Aβ1–40 E22Δ had a significant neurotoxic effect in comparison to controls (***$P<0.001$; Tukey's test), whereas Aβ1–42 E22Δ and Aβ1–40 wt were not significantly toxic. Error bars indicate error propagation.

(Fig. 6a–e). NeuriteTracer analysis revealed significantly decreased lengths of neurites ($P<0.001$; Tukey's test) following incubation with either Aβ1–42 wt or Aβ1–42 E22Δ (Fig. 6f). Additionally, there was a detectable difference in the light microscopic pattern of Aβ immunoreactivity varying from punctate Aβ1–40 wt, over web-like Aβ1–40 E22Δ, to plaque-resembling Aβ1–42 wt and Aβ1–42 E22Δ. In addition, Aβ staining was only observed on the surface of the cells (cf. Supplementary Data).

Fibrils of Aβ1–40 E22Δ and Aβ1–42 E22Δ bind the amyloid tracer PIB with similar efficiency relative to Aβ wt peptides

Previous brain imaging studies on a patient bearing the E22Δ mutation with positron emission tomography[5] had been interpreted such that Aβ E22Δ peptides have either no tendency or only a low tendency of forming amyloid deposits *in vivo* based on a low *in vivo* retention signal of the amyloid-specific tracer [^{11}C]Pittsburgh compound B ([^{11}C]

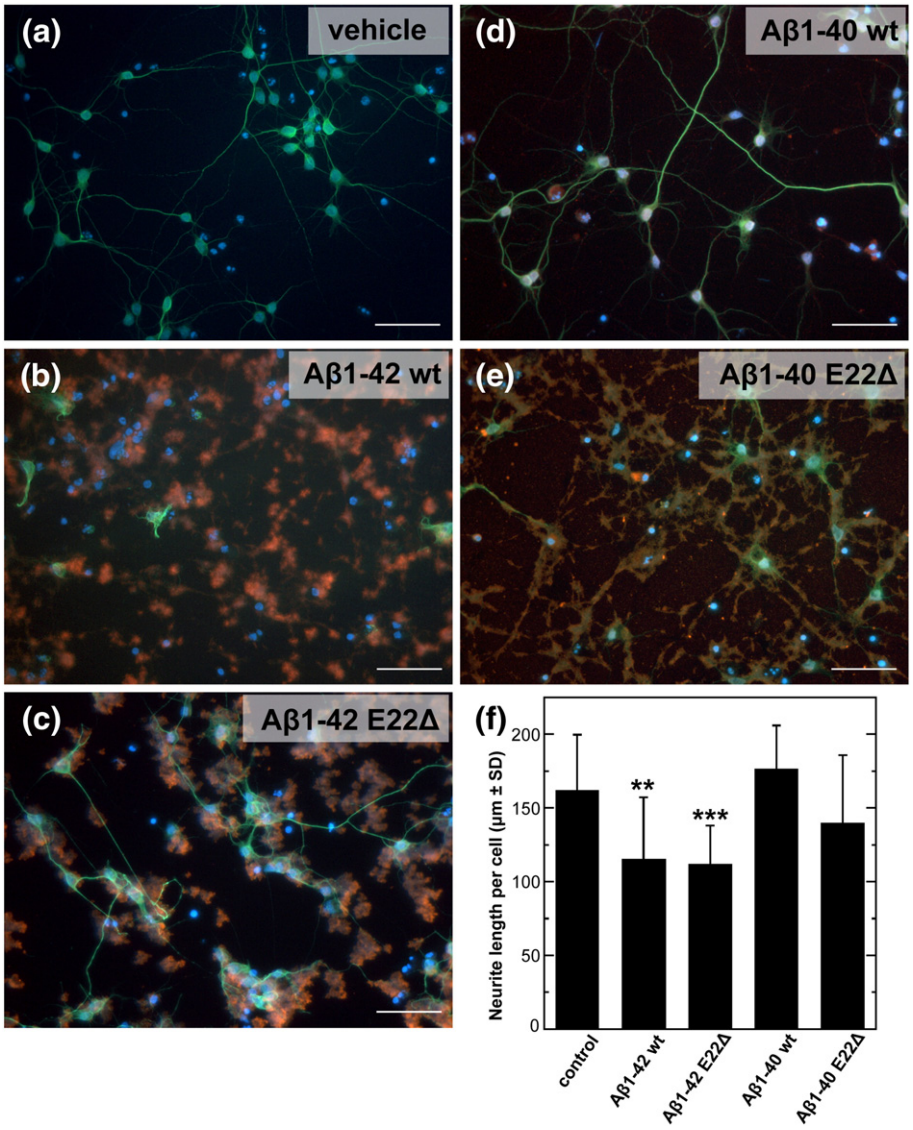

Fig. 6. Morphology of the neuronal cell cultures after incubation with the Aβ variants. Primary neuronal cell cultures were exposed to a vehicle control only (a) or to recombinant Aβ1–42 wt (b), Aβ1–42 E22Δ (c), Aβ1–40 wt (d), and Aβ1–40 E22Δ (e) for 72 h, and were labeled for MAP-2 (green), cell nuclei (DAPI; blue), and Aβ (red). A significant decrease in neurite length per living cell was determined using NeuriteTracer analysis for Aβ1–42 wt (**$P<0.01$; Tukey's test) and Aβ1–42 E22Δ (***$P<0.001$; Tukey's test) (f). Different Aβ variants deposited on the coverslips formed different patterns, varying from punctate (Aβ1–40 wt), over web like (Aβ1–40 E22Δ), to plaque resembling (Aβ1–42 wt and Aβ1–42 E22Δ) (scale bar represents 50 μm).

PIB). As this observation is in contrast to the increased tendency of amyloid fibril formation for the Aβ E22Δ peptides *in vitro* (Figs. 2 and 3), we investigated whether this discrepancy might be caused by a weaker affinity of Aβ E22Δ fibrils for [^{11}C]PIB. Using the nonradioactive analogue of [^{11}C]PIB, 6-benzothiazolol (6-OH-BTA-1), we quantified the 6-OH-BTA-1 binding capacity of fibrils formed by all four Aβ peptides by incubation of preformed fibrils with identical 6-OH-BTA-1 concentrations (5 μM) for 20 min at pH 7.4 and 37 °C, followed by the separation of free dye and fibril-bound dye by ultracentrifugation and the measurement of the remaining dye-specific fluorescence intensity in the supernatants. 6-OH-BTA-1 already exhibited a significant fluorescence in the absence of fibrils (fluorescence maximum at 428 nm) that decreased in the presence of fibrils (Supplementary Data). In addition, in contrast to thioflavin T, binding of 6-OH-BTA-1 to the fibrils only caused minor shifts in the fluorescence maximum of the dye (Fig. 7a). The binding stoichiometry of 6-OH-BTA-1 per Aβ monomer in the fibrils was found to be around 1:4 for Aβ1–42 wt fibrils, 1:10 for Aβ1–40 wt, 1:5 for Aβ1–42 E22Δ, and 1:6 for Aβ1–40 E22Δ (Fig. 7b). Fibrils of Aβ1–40 E22Δ and Aβ1–42 E22Δ thus showed a 1.7-fold higher and a 1.3-fold lower dye binding capacity than the corresponding wt fibrils, respectively. The results demonstrate that both Aβ peptides with the deletion E22Δ retain the ability of binding [^{11}C]PIB. Consequently, the low *in vivo* amyloid staining intensity for the E22Δ FAD patient reported by Tomiyama *et al.* is indeed most likely indicative of low *in vivo* concentrations of amyloid deposits composed of Aβ peptides with the E22Δ mutation.[5]

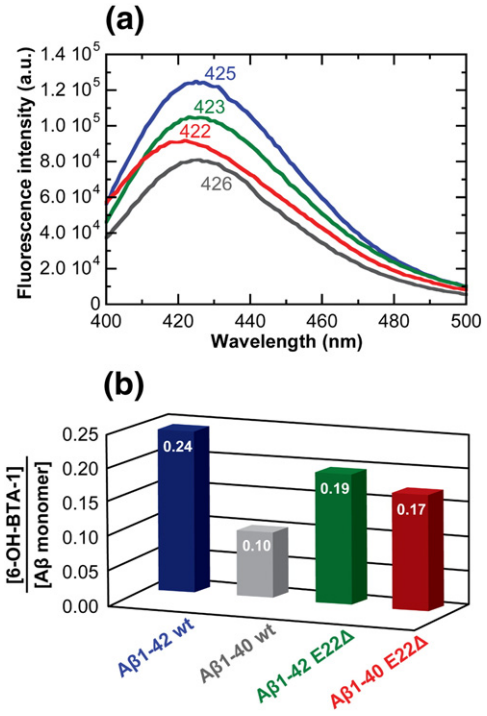

Fig. 7. (a) Fluorescence emission spectra of 6-OH-BTA-1 (λ_{ex} = 352 nm) bound to fibrils of Aβ1–42 wt (blue line), Aβ1–40 wt (gray line), Aβ1–42 E22Δ (green line), and Aβ1–40 E22Δ (red line) (identical total Aβ monomer concentrations: 10 μM). The corresponding fluorescence maxima are indicated with the same color code. (b) Comparison of the 6-OH-BTA-1 binding capacity of the four different Aβ fibrils. Dye binding capacities are expressed as the average number of dye molecules bound per Aβ monomer in the fibrils.

Discussion

In this study, we showed that the novel FAD mutation in the APP gene corresponding to the deletion of E22 within the Aβ sequence favors Aβ fibril formation *in vitro*. Fibril formation recorded by the increase in thioflavin T fluorescence and analysis of soluble Aβ content revealed a significantly higher aggregation propensity of Aβ1–42 E22Δ compared to wt Aβ1–42. In addition, we demonstrated that Aβ1–40 E22Δ forms a hitherto unknown type of Aβ fibrils, characterized by a 6-fold to 7-fold increased fluorescence of fibril-bound thioflavin T, more hydrophobic thioflavin T binding sites, and a strongly increased tendency of forming fibrillar bundles relative to fibrils of Aβ1–40 wt and Aβ1–42 wt. Despite the widespread use of thioflavin T for monitoring amyloid fibril formation, the mechanism of its binding to amyloid fibrils is still not well understood.[23,24] It was suggested that the development of the fibril-specific fluorescence increase in thioflavin T requires cavities of appropriate diameter and length.[25] The thioflavin T binding sites in amyloid fibrils of insulin were proposed to be located between the protofilaments forming the protofibrils or between the protofibrils forming the mature fibrils.[26] As fibrils of Aβ1–40 E22Δ showed a strong tendency of forming bundle-like assemblies, their increased apparent thioflavin T binding capacity could be a result of the creation of additional thioflavin T binding sites in the contact areas between adjacent fibrils in the bundles. Notably, formation of the novel type of fibrils observed for Aβ1–40 E22Δ is inhibited by the presence of Aβ residues 41 and 42 in Aβ1–42 E22Δ.

The exact three-dimensional structure of Aβ fibrils has not been determined so far, but different models for the structure of Aβ fibrils have been proposed. Regarding the secondary structure context of residue E22, Lührs *et al.*[27] and Petkova *et al.*[28] proposed that it lies in a β-strand, while models of Morimoto *et al.*[29] and Williams *et al.*[30] suggested that E22 is contained in a segment of irregular secondary structure between β-strands. The presence of a

turn structure at positions 22 and 23 was also verified for Aβ with the Italian mutation (E22K).[31] If one assumes that E22 is contained in a β-strand in the fibrils of Aβ1–40 wt, the simplest explanation for the generation of an entirely different fibril type in the case of Aβ1–40 E22Δ would be that the β-strand segment containing residue 22 is inverted by 180° through the E22 deletion (which would cause an entirely different pattern of side-chain alignment in adjacent Aβ monomers of Aβ1–40 E22Δ fibrils) or that the β-strand is interrupted after residue 21. The ability of Aβ1–40 E22Δ to form a previously unknown type of Aβ fibril is also consistent with the observation that even fibrils of Aβ1–40 wt are capable of forming at least 12 different types of fibrillar quaternary structures under identical aggregation conditions.[32,33]

Our results on the aggregation kinetics of Aβ1–40 E22Δ and Aβ1–42 E22Δ are in contrast to previous *in vitro* aggregation studies in which no fibril formation of synthetic Aβ E22Δ was observed.[5] We can only speculate about the reasons for this discrepancy, but a possible explanation could be the presence of 5–9% impurities contained in the synthetic Aβ peptides with the E22 deletion used by Tomiyama *et al.*[5] We showed recently that even smaller amounts of impurities in synthetic Aβ preparations in the range of 3% can significantly slow the rate of spontaneous Aβ amyloid fibril formation *in vitro*, possibly by preventing further fibril growth after the incorporation of synthetic side products into the growing fibril ends that are similar to Aβ wt in their covalent structure.[22] A fraction of 5–9% impurities may thus have prevented the aggregation of Aβ1–40 E22Δ and Aβ1–42 E22Δ in the study of Tomiyama *et al.*[5]

Our results are in agreement with previous studies on charge alterations within the Aβ sequence, where a change or a loss of charge at position 22 in Aβ enhanced both the aggregation propensity and the toxicity of the corresponding mutant peptides.[34,35] Aβ variants corresponding to the FAD mutations Dutch (E22Q), Italian (E22K), and Arctic (E22G) aggregated much faster than wt Aβ.[12,36,37] We found that the Aβ1–42 E22Δ showed an increased tendency of β-sheet conformation and aggregated faster than Aβ1–42 wt. This agrees with the faster rate of Aβ amyloid formation at acidic pH compared to neutral or basic pH,[38,39] where the E22 side chain is less negatively charged, and to an increased aggregation rate of Aβ peptides with the Dutch mutation (E22Q), where the barrier of Aβ monomer incorporation into growing fibrils was lowered.[40] We showed that Aβ1–42 E22Δ, which lacks the polar glutamate 22, tends to form β-sheet structure even in 10 mM NaOH, whereas the wt peptide adopts random-coil conformation. Fraser *et al.* observed the same effect for the Dutch variant of Aβ (E22Q) with Fourier transform infrared spectroscopy.[39] We also recorded the far-UV CD spectra of Aβ variants at pH 7.4 directly after mixing Aβ with the buffer at 25 °C instead of 37 °C, which slowed the aggregation reactions and allowed an analysis of the state of Aβ close to the aggregation start. The spectrum of Aβ1–42 E22Δ confirmed the rapid formation of β-sheet structure, while Aβ1–40 E22Δ and the wt peptides still predominantly showed random-coil conformation (Supplementary Data).

Tomiyama *et al.* suggested that both Aβ1–40 E22Δ and Aβ1–42 E22Δ do not form fibrils *in vivo*, as the retention signal of [^{11}C]PIB was lower in the brain of a homozygous patient bearing the Osaka mutation than in the brain of another patient with sporadic AD.[5] To exclude that the lower [^{11}C]PIB retention signal in the patient with the E22Δ mutation was caused by the inability of Aβ E22Δ fibrils to bind [^{11}C]PIB, we quantified the [PIB]/[Aβ monomer] ratio in fibrils formed by wt Aβ and the variants with the E22 deletion. The results showed that both fibrils of Aβ1–40 E22Δ and Aβ1–42 E22Δ had a PIB binding capacity similar to Aβ1–42 wt fibrils. As the examined FAD patient bearing the Osaka mutation still showed a low [^{11}C]PIB retention signal compared to a negative control,[5] and as both Aβ1–40 E22Δ and Aβ1–42 E22Δ do form amyloid fibrils, we believe that the question of whether or not E22Δ mutation carriers accumulate Aβ amyloid in the brain is still unsolved and needs to be examined further. Notably, Aβ1–42 wt fibrils exhibited a more than 2-fold higher PIB binding capacity compared to Aβ1–40 wt fibrils. Assuming that Aβ1–42 wt is the main amyloidogenic species *in vivo*,[6] this result could also explain the efficiency of PIB in the *in vivo* visualization of Aβ amyloid deposits.

To investigate the pathogenic role of the E22Δ mutation, we performed neurotoxicity assays and immunocytochemical imaging of cultured rat primary neurons treated with the four Aβ variants. Whereas Aβ1–42 wt caused significant toxic effects on neuronal viability and morphology and as Aβ1–40 wt had no effect, the E22Δ mutation rendered Aβ1–40 E22Δ neurotoxic. This would agree with previous studies showing that both inversion (E22K) and loss (E22A and E22Q) of charge of glutamate 22 increased the toxicity of the Aβ peptide towards cultured human cerebrovascular smooth muscle cells compared to Aβ wt or the charge-preserving variant Aβ E22D.[35] In contrast to Aβ1–40 E22Δ, Aβ1–42 E22Δ did not affect cell viability under our tested conditions. However, it decreased neurite outgrowth in neuronal primary cultures. A large body of evidence shows that the earlier stages of AD are best characterized by synaptic loss and reduction in neuronal processes, followed much later by neuronal death. Our results on neurite outgrowth are in good agreement with earlier data demonstrating that Aβ1–42 E22Δ indeed causes a more

potent synaptotoxic effect but lower neurodegeneration than wt peptide.[18] The survival of all neurons upon treatment with Aβ1–42 E22Δ may be explained by the rapid and complete aggregation of Aβ1–42 E22Δ into fibrils without a significant accumulation of toxic oligomers. This would be reminiscent of Aβ1–42 with the Arctic mutation (E22G) that also shows fast aggregation *in vitro* and promotes the formation of prominent amyloid plaques *in vivo* but does not cause behavioral deficits in ARC6 mice expressing the Arctic Aβ.[41] Further experiments would certainly be required to identify the mechanism underlying the nontoxicity of Aβ1–42 E22Δ.

Aβ1–40 is the major Aβ form present *in vivo*, with an about 10-fold higher concentration compared to Aβ1–42,[4] and a corresponding *in vivo* excess of Aβ1–40 E22Δ over Aβ1–42 E22Δ has also been confirmed for FAD patients bearing the Osaka mutation.[5] The significant toxicity of Aβ1–40 E22Δ compared to nontoxic Aβ1–40 wt may thus explain the early onset of dementia caused by the E22Δ mutation in Osaka FAD patients. Furthermore, the decreased neurite outgrowth in neuronal primary cultures treated with Aβ1–42 E22Δ indicates that a synaptotoxic effect could play an important role in the initiation of early-onset dementia in patients with this mutation. Further *in vivo* and *in vitro* studies on the effects of Aβ1–40 E22Δ and Aβ1–42 E22Δ are necessary to elucidate the pathogenic significance of the E22Δ mutation.

Materials and Methods

Plasmids and protein production

The plasmids for the expression of wt Aβ1–40 and wt Aβ1–42 in *Escherichia coli* as fusions to the peptide sequence $(NANP)_{19}$ with an N-terminal hexahistidine tag have been described previously.[22] The deletion of codon 22 in both Aβ1–40 and Aβ1–42 was performed with the QuikChange site-directed mutagenesis kit (Stratagene). The correct genetic sequences of the constructs were verified by dideoxynucleotide DNA sequencing. Aβ production was based on the expression of Aβ as a fusion protein and the subsequent cleavage of the fusion protein with tobacco etch virus protease, as described earlier for Aβ1–40 wt and Aβ1–42 wt.[22] Briefly, the fusion proteins were expressed in *E. coli* BL21(DE3) under T7 promoter control, and cells were induced at OD_{600} ~3.5 for 4 h at 37 °C with 1 mM IPTG. The cells were harvested and resuspended in 20 mM H_3PO_4–NaOH, 6 M guanidinium chloride, and 0.3 M NaCl (pH 8.0; buffer A), and the suspension was ultracentrifuged after incubation at 4 °C for 90 min. The supernatant was diluted with buffer A containing 500 mM imidazole–HCl to a concentration of 10 mM imidazole and loaded on a Ni^{2+}-NTA agarose column. After a wash with buffer A containing 10 mM imidazole–HCl, the fusion proteins were eluted with buffer A containing 250 mM imidazole–HCl and further purified via reversed-phase high-performance liquid chromatography at 80 °C in aqueous acetonitrile (ACN) containing 0.1% trifluoroacetic acid on a Zorbax SB300 C8 column (Agilent). The fusion proteins were eluted isocratically at ACN concentrations of 28–30.5% and lyophilized. Cleavage of the fusion proteins (100 μM) with 7.5 μM tobacco etch virus protease was performed in 10 mM Tris–HCl (pH 8.0), 0.5 mM ethylenediaminetetraacetic acid, and 1 mM DTT (buffer B) for 1 h at room temperature, followed by incubation at 4 °C overnight. The cleaved Aβ peptides precipitated during the cleavage reactions. They were pelleted by centrifugation (4500*g*, 20 min, 4 °C), dissolved in 6 M guanidinium chloride–HCl (pH 2.0), and purified via reversed-phase high-performance liquid chromatography, as described above. Aβ1–40 and Aβ1–40 E22Δ were eluted at 28% ACN, and Aβ1–42 and Aβ1–42 E22Δ were eluted at 30.5% ACN. The eluted peptides were aliquoted in Protein LoBind Eppendorf tubes (Vaudaux-Eppendorf), lyophilized, and stored at −80 °C. The high purity and identity of the peptides were verified by matrix-assisted laser desorption/ionization time-of-flight mass spectrometry using sinapinic acid as matrix (data not shown).

Preparation of Aβ solutions

The Aβ variants were dissolved in 10 mM NaOH to concentrations of 100–150 μM and subjected to ultracentrifugation for 1 h at 135,500*g* and 4 °C. The Aβ concentration in the supernatant was determined via the absorbance of Aβ at 280 nm in 10 mM NaOH (extinction coefficient at 280 nm and pH 12 corresponding to a single tyrosine residue: 1730 M^{-1} cm^{-1}).[22] The stock solutions were kept on ice and used for aggregation experiments within 24 h.

Aβ aggregation reactions followed via thioflavin T fluorescence

Aggregation reactions were performed at 37 °C with 7.5 μM Aβ (final concentration) in 10 mM H_3PO_4–NaOH (pH 7.4), 100 mM NaCl, and 35 μM thioflavin T in a volume of 750 μl in stirred quartz fluorescence cuvettes (1 cm × 0.4 cm). The thioflavin T concentration was determined via its extinction coefficient of 36,000 M^{-1} cm^{-1} at 412 nm.[25,42] The presence of thioflavin T from the beginning of the aggregation reaction was verified to have no influence on aggregation kinetics or thioflavin T fluorescence intensity compared to the addition of thioflavin T to reaction aliquots removed after different time points of the reaction. Aggregation reactions were started by a dilution of the Aβ stock solution in 10 mM NaOH (prepared and ultracentrifuged immediately before use) with an aggregation buffer mix, resulting in pH 7.4 and the final concentrations indicated above. Since newly formed Aβ fibrils have a tendency to float at the surface of the solution, the reactions were stirred (magnetic stirrer) at 1000 rpm using bidirectional (autoreversing) stirring with fast acceleration (Electronic Stirrer 300; Rank Brothers Ltd.), which guaranteed a homogeneous fibril suspension throughout the reaction and allowed continuous recording of thioflavin T fluorescence. Thioflavin T fluorescence emission at 482 nm (excitation at 440 nm; excitation and

emission slit: 1.6 nm) was monitored on a Quantamaster (QM-7/2003) fluorescence spectrometer (Photon Technology International) every 30 s for 10 s and averaged automatically. Thioflavin T fluorescence spectra were recorded in the range of 450–550 nm (excitation at 440 nm) after the fluorescence at 482 nm had reached its maximum in the aggregation reactions, and corrected for the buffer.

Quantification of soluble Aβ during aggregation

Aggregation reactions were performed as described above, but without thioflavin T (thioflavin T was verified to have no influence on Aβ aggregation kinetics). At different time points, aliquots of the aggregation reactions were removed, quenched by rapid cooling on ice, and ultracentrifuged (135,500*g*, 40 min, 4 °C). The supernatants were mixed with 100 mM NaOH, and the concentration of soluble Aβ was measured via absorbance at 220 nm.

Binding of 6-OH-BTA-1 to Aβ fibrils

6-OH-BTA-1 was purchased from ABX Advanced Biochemical Compounds GmbH (Germany) and dissolved in dimethyl sulfoxide (DMSO) to a final concentration of 1 mM. The fluorescence excitation and emission spectra of 5 μM 6-OH-BTA-1 were recorded in 10 mM H_3PO_4–NaOH (pH 7.4), 100 mM NaCl, and 0.5% DMSO in a Quantamaster (QM-7/2003) fluorescence spectrometer (Photon Technology International). Aβ fibrils were formed in 10 mM H_3PO_4–NaOH (pH 7.4) and 100 mM NaCl at 37 °C (final Aβ concentration: 10 μM). The resulting Aβ fibril suspension (900 μl) was mixed with 4.5 μl of 6-OH-BTA-1 (final concentration: 5 μM in 0.5% DMSO) and incubated in a Thermomixer for 20 min at 37 °C and 750 rpm to allow binding of 6-OH-BTA-1 to the fibrils. The fluorescence spectra of these reaction mixtures were recorded at 23 °C (excitation at 352 nm; emission range of 400–500 nm). The reaction mixtures were then centrifuged at 135,500*g* and 20 °C for 15 min. The spectra of fibril-bound dye were recorded after resuspending the pellets in the original buffer volume, and unbound dye was quantified via fluorescence at 428 nm of the remaining dye in the supernatant. 6-OH-BTA-1 was verified to show a linear dependence of fluorescence intensity on concentration in the range of 0.08–5 μM.

CD spectroscopy

Far-UV CD spectra were recorded on a Jasco J-715 spectropolarimeter (using a cuvette with a path length of 0.2 mm), accumulated 20 times, averaged, and corrected for the buffer. We recorded the spectra of 75 μM Aβ in 10 mM NaOH after ultracentrifugation for 1 h at 135,500*g* and 4 °C.

Electron microscopy

Samples of Aβ fibrils were removed from the aggregation reactions after the maximum thioflavin T fluorescence had been reached and applied to carbon-coated copper grids (Quantifoil Micro Tools GmbH) for 1 min, washed with water, and stained with 2% uranyl acetate for 30 s. Electron micrographs were recorded at 100 MeV on a FEI Morgagni 268 transmission electron microscope. Thioflavin T was verified to have no influence on the appearance/morphology of the fibrils.

Rat primary cortical neuron cultures

Rat primary cortical neuron cultures were prepared from the cortices of embryonic 18-day (E18) Wistar rats. Cortices were dissected out, exposed for 10 min to 2.4 U/ml Dispase II (Roche Applied Science), and triturated to isolate cells. Neurons were plated in neurobasal medium with B-27 supplements (GIBCO, Invitrogen) on 24-well plates. The plates contained glass coverslips precoated with poly-L-ornithine (Sigma-Aldrich). Cells were plated at a density of 48,500 cells/cm^2 and grown in a humidified incubator at 7% CO_2.

Cytotoxicity assays and immunocytochemistry

Primary cortical neuron cultures were treated with Aβ or vehicle control on DIV 5 for 72 h. Aβ (94 μM in 10 mM NaOH) was rapidly mixed on ice with buffer, resulting in a solution of 75 μM Aβ in 10 mM H_3PO_4–NaOH (pH 7.4) and 10 mM NaCl. This solution was immediately mixed with the cell culture medium such that the final Aβ concentration in the medium was 7.5 μM. Unless otherwise indicated, toxicity data were acquired from at least two independent experiments. Cytotoxicity was assessed by measuring the activity of the cytosolic enzyme LDH released into the culture medium according to the manufacturer's protocol (*In Vitro* Toxicology Assay Kit, Lactic Dehydrogenase Based; Sigma-Aldrich). Briefly, half of the volume of the culture medium was collected from a culture well after treatment with Aβ for 72 h and incubated with an equal volume of the LDH substrate solution for 30 min. LDH activity was quantified via absorbance at 490 nm. Cell morphology studies were based on the staining of cultures fixed with 4% (wt/vol) paraformaldehyde (15 min at room temperature) using mouse anti-MAP-2 antibody (1:1000; Sigma), anti-Aβ-peptide antibody recognizing the N-terminal part of Aβ (1:500; Zymed, Invitrogen), and 4′,6-diamidino-2-phenylindole (DAPI). Fluorescence microscopy analysis was performed on a Leica DM IRE2 microscope equipped with a Leica DFC480 camera. Neurite lengths and the amount of living cells were determined by the application NeuriteTracer for the multiplatform image processing program ImageJ.[43] The results were expressed as neurite length per cell for each treatment. Each readout per well was averaged from the images of five visual fields.

Supplementary materials related to this article can be found online at doi:10.1016/j.jmb.2011.02.049

Acknowledgements

We would like to thank Serge Chesnov (FGCZ) for matrix-assisted laser desorption/ionization time-of-

flight mass spectrometry analysis. We acknowledge the technical support of the Electron Microscopy Center of ETH Zurich (EMEZ). This work was funded by the ETH Zurich, the University of Zurich, and the Swiss National Science Foundation in the framework of NCCR 'Neural Plasticity and Repair.'

References

1. Hardy, J. & Selkoe, D. J. (2002). The amyloid hypothesis of Alzheimer's disease: progress and problems on the road to therapeutics. *Science*, **297**, 353–356.
2. Selkoe, D. J. (2004). Cell biology of protein misfolding: the examples of Alzheimer's and Parkinson's diseases. *Nat. Cell Biol.* **6**, 1054–1061.
3. Suzuki, N., Cheung, T. T., Cai, X. D., Odaka, A., Otvos, L., Jr, Eckman, C. *et al.* (1994). An increased percentage of long amyloid beta protein secreted by familial amyloid beta protein precursor (beta APP717) mutants. *Science*, **264**, 1336–1340.
4. Jensen, M., Schroder, J., Blomberg, M., Engvall, B., Pantel, J., Ida, N. *et al.* (1999). Cerebrospinal fluid A beta42 is increased early in sporadic Alzheimer's disease and declines with disease progression. *Ann. Neurol.* **45**, 504–511.
5. Tomiyama, T., Nagata, T., Shimada, H., Teraoka, R., Fukushima, A., Kanemitsu, H. *et al.* (2008). A new amyloid beta variant favoring oligomerization in Alzheimer's-type dementia. *Ann. Neurol.* **63**, 377–387.
6. Irie, K., Murakami, K., Masuda, Y., Morimoto, A., Ohigashi, H., Ohashi, R. *et al.* (2005). Structure of beta-amyloid fibrils and its relevance to their neurotoxicity: implications for the pathogenesis of Alzheimer's disease. *J. Biosci. Bioeng.* **99**, 437–447.
7. Sherrington, R., Rogaev, E. I., Liang, Y., Rogaeva, E. A., Levesque, G., Ikeda, M. *et al.* (1995). Cloning of a gene bearing missense mutations in early-onset familial Alzheimer's disease. *Nature*, **375**, 754–760.
8. Levy-Lahad, E., Wasco, W., Poorkaj, P., Romano, D. M., Oshima, J., Pettingell, W. H. *et al.* (1995). Candidate gene for the chromosome 1 familial Alzheimer's disease locus. *Science*, **269**, 973–977.
9. Hendriks, L., van Duijn, C. M., Cras, P., Cruts, M., Van Hul, W., van Harskamp, F. *et al.* (1992). Presenile dementia and cerebral haemorrhage linked to a mutation at codon 692 of the beta-amyloid precursor protein gene. *Nat. Genet.* **1**, 218–221.
10. Levy, E., Carman, M. D., Fernandez-Madrid, I. J., Power, M. D., Lieberburg, I., van Duinen, S. G. *et al.* (1990). Mutation of the Alzheimer's disease amyloid gene in hereditary cerebral hemorrhage, Dutch type. *Science*, **248**, 1124–1126.
11. Tagliavini, F., Rossi, G., Padovani, A., Magoni, M., Andora, G., Sgarzi, M. *et al.* (1999). A new βPP mutation related to hereditary cerebral haemorrhage. *Alzheimer's Rep.* **2**, S28.
12. Nilsberth, C., Westlind-Danielsson, A., Eckman, C. B., Condron, M. M., Axelman, K., Forsell, C. *et al.* (2001). The 'Arctic' APP mutation (E693G) causes Alzheimer's disease by enhanced Abeta protofibril formation. *Nat. Neurosci.* **4**, 887–893.
13. Grabowski, T. J., Cho, H. S., Vonsattel, J. P., Rebeck, G. W. & Greenberg, S. M. (2001). Novel amyloid precursor protein mutation in an Iowa family with dementia and severe cerebral amyloid angiopathy. *Ann. Neurol.* **49**, 697–705.
14. Wakutani, Y., Watanabe, K., Adachi, Y., Wada-Isoe, K., Urakami, K., Ninomiya, H. *et al.* (2004). Novel amyloid precursor protein gene missense mutation (D678N) in probable familial Alzheimer's disease. *J. Neurol. Neurosurg. Psychiatry*, **75**, 1039–1042.
15. Janssen, J. C., Beck, J. A., Campbell, T. A., Dickinson, A., Fox, N. C., Harvey, R. J. *et al.* (2003). Early onset familial Alzheimer's disease: mutation frequency in 31 families. *Neurology*, **60**, 235–239.
16. Di Fede, G., Catania, M., Morbin, M., Rossi, G., Suardi, S., Mazzoleni, G. *et al.* (2009). A recessive mutation in the APP gene with dominant-negative effect on amyloidogenesis. *Science*, **323**, 1473–1477.
17. Finder, V. H. & Glockshuber, R. (2007). Amyloid-beta aggregation. *Neurodegener. Dis.* **4**, 13–27.
18. Takuma, H., Teraoka, R., Mori, H. & Tomiyama, T. (2008). Amyloid-beta E22Delta variant induces synaptic alteration in mouse hippocampal slices. *NeuroReport*, **19**, 615–619.
19. Tomiyama, T., Matsuyama, S., Iso, H., Umeda, T., Takuma, H., Ohnishi, K. *et al.* (2010). A mouse model of amyloid beta oligomers: their contribution to synaptic alteration, abnormal tau phosphorylation, glial activation, and neuronal loss *in vivo*. *J. Neurosci.* **30**, 4845–4856.
20. Nishitsuji, K., Tomiyama, T., Ishibashi, K., Ito, K., Teraoka, R., Lambert, M. P. *et al.* (2009). The E693Delta mutation in amyloid precursor protein increases intracellular accumulation of amyloid beta oligomers and causes endoplasmic reticulum stress-induced apoptosis in cultured cells. *Am. J. Pathol.* **174**, 957–969.
21. Nagata, T., Tominaga, T., Mori, H., Yaguchi, T. & Nishizaki, T. (2010). DCP-LA neutralizes mutant amyloid beta peptide-induced impairment of long-term potentiation and spatial learning. *Behav. Brain Res.* **206**, 151–154.
22. Finder, V. H., Vodopivec, I., Nitsch, R. M. & Glockshuber, R. (2010). The recombinant amyloid-beta peptide Abeta1–42 aggregates faster and is more neurotoxic than synthetic Abeta1–42. *J. Mol. Biol.* **396**, 9–18.
23. Wu, C., Wang, Z., Lei, H., Duan, Y., Bowers, M. T. & Shea, J. E. (2008). The binding of thioflavin T and its neutral analog BTA-1 to protofibrils of the Alzheimer's disease Abeta(16–22) peptide probed by molecular dynamics simulations. *J. Mol. Biol.* **384**, 718–729.
24. Khurana, R., Coleman, C., Ionescu-Zanetti, C., Carter, S. A., Krishna, V., Grover, R. K. *et al.* (2005). Mechanism of thioflavin T binding to amyloid fibrils. *J. Struct. Biol.* **151**, 229–238.
25. Groenning, M., Olsen, L., van de Weert, M., Flink, J. M., Frokjaer, S. & Jorgensen, F. S. (2007). Study on the binding of thioflavin T to beta-sheet-rich and non-beta-sheet cavities. *J. Struct. Biol.* **158**, 358–369.
26. Groenning, M., Norrman, M., Flink, J. M., van de Weert, M., Bukrinsky, J. T., Schluckebier, G. & Frokjaer, S. (2007). Binding mode of thioflavin T in insulin amyloid fibrils. *J. Struct. Biol.* **159**, 483–497.

27. Lührs, T., Ritter, C., Adrian, M., Riek-Loher, D., Bohrmann, B., Dobeli, H. *et al.* (2005). 3D structure of Alzheimer's amyloid-beta(1–42) fibrils. *Proc. Natl Acad. Sci. USA*, **102**, 17342–17347.
28. Petkova, A. T., Ishii, Y., Balbach, J. J., Antzutkin, O. N., Leapman, R. D., Delaglio, F. & Tycko, R. (2002). A structural model for Alzheimer's beta-amyloid fibrils based on experimental constraints from solid state NMR. *Proc. Natl Acad. Sci. USA*, **99**, 16742–16747.
29. Morimoto, A., Irie, K., Murakami, K., Masuda, Y., Ohigashi, H., Nagao, M. *et al.* (2004). Analysis of the secondary structure of beta-amyloid (Abeta42) fibrils by systematic proline replacement. *J. Biol. Chem.* **279**, 52781–52788.
30. Williams, A. D., Portelius, E., Kheterpal, I., Guo, J. T., Cook, K. D., Xu, Y. & Wetzel, R. (2004). Mapping Abeta amyloid fibril secondary structure using scanning proline mutagenesis. *J. Mol. Biol.* **335**, 833–842.
31. Masuda, Y., Irie, K., Murakami, K., Ohigashi, H., Ohashi, R., Takegoshi, K. *et al.* (2005). Verification of the turn at positions 22 and 23 of the beta-amyloid fibrils with Italian mutation using solid-state NMR. *Bioorg. Med. Chem.* **13**, 6803–6809.
32. Meinhardt, J., Sachse, C., Hortschansky, P., Grigorieff, N. & Fandrich, M. (2009). Abeta(1–40) fibril polymorphism implies diverse interaction patterns in amyloid fibrils. *J. Mol. Biol.* **386**, 869–877.
33. Fändrich, M., Meinhardt, J. & Grigorieff, N. (2009). Structural polymorphism of Alzheimer Abeta and other amyloid fibrils. *Prion*, **3**, 89–93.
34. Kim, W. & Hecht, M. H. (2008). Mutations enhance the aggregation propensity of the Alzheimer's A beta peptide. *J. Mol. Biol.* **377**, 565–574.
35. Melchor, J. P., McVoy, L. & Van Nostrand, W. E. (2000). Charge alterations of E22 enhance the pathogenic properties of the amyloid beta-protein. *J. Neurochem.* **74**, 2209–2212.
36. Clements, A., Walsh, D. M., Williams, C. H. & Allsop, D. (1993). Effects of the mutations Glu22 to Gln and Ala21 to Gly on the aggregation of a synthetic fragment of the Alzheimer's amyloid beta/A4 peptide. *Neurosci. Lett.* **161**, 17–20.
37. Miravalle, L., Tokuda, T., Chiarle, R., Giaccone, G., Bugiani, O., Tagliavini, F. *et al.* (2000). Substitutions at codon 22 of Alzheimer's Abeta peptide induce diverse conformational changes and apoptotic effects in human cerebral endothelial cells. *J. Biol. Chem.* **275**, 27110–27116.
38. Kirkitadze, M. D., Condron, M. M. & Teplow, D. B. (2001). Identification and characterization of key kinetic intermediates in amyloid beta-protein fibrillogenesis. *J. Mol. Biol.* **312**, 1103–1119.
39. Fraser, P. E., Nguyen, J. T., Inouye, H., Surewicz, W. K., Selkoe, D. J., Podlisny, M. B. & Kirschner, D. A. (1992). Fibril formation by primate, rodent, and Dutch-hemorrhagic analogues of Alzheimer amyloid beta-protein. *Biochemistry*, **31**, 10716–10723.
40. Baumketner, A., Krone, M. G. & Shea, J. E. (2008). Role of the familial Dutch mutation E22Q in the folding and aggregation of the 15–28 fragment of the Alzheimer amyloid-beta protein. *Proc. Natl Acad. Sci. USA*, **105**, 6027–6032.
41. Cheng, I. H., Scearce-Levie, K., Legleiter, J., Palop, J. J., Gerstein, H., Bien-Ly, N. *et al.* (2007). Accelerating amyloid-beta fibrillization reduces oligomer levels and functional deficits in Alzheimer disease mouse models. *J. Biol. Chem.* **282**, 23818–23828.
42. De Ferrari, G. V., Mallender, W. D., Inestrosa, N. C. & Rosenberry, T. L. (2001). Thioflavin T is a fluorescent probe of the acetylcholinesterase peripheral site that reveals conformational interactions between the peripheral and acylation sites. *J. Biol. Chem.* **276**, 23282–23287.
43. Pool, M., Thiemann, J., Bar-Or, A. & Fournier, A. E. (2008). NeuriteTracer: a novel ImageJ plugin for automated quantification of neurite outgrowth. *J. Neurosci. Methods*, **168**, 134–139.

Note added in proof: After acceptance of this manuscript, we learned that a parallel study on synthetic Aβ1–40 E22Δ was published (Cloe A. L., Orgel, J. P. R. O., Sachleben, J. R., Tycko, R. & Meredith, S. C. (2011). *Biochemistry*, **50**, 2026–2039). Cloe et al. also demonstrated that Aβ1–40 E22Δ is capable of forming amyloid fibrils which differ from fibrils of wt Aβ1–40. The fibrils of synthetic Aβ1–40 E22Δ however showed lower thioflavin T binding capacity relative to wt Aβ1–40 fibrils, while our results on recombinant Aβ1–40 E22Δ fibrils revealed strongly increased thioflavin T binding. The reasons for these differences need to be investigated further.